Journal of Digital Imaging
https://doi.org/10.1007/s10278-022-00667-y

FWLICM-Deep Learning: Fuzzy Weighted Local Information C-Means Clustering-Based Lung Lobe Segmentation with Deep Learning for COVID-19 Detection

R. Rajeswari[1] · Veerraju Gampala[2] · Balajee Maram[3] · R. Cristin[4]

Received: 14 September 2021 / Revised: 26 April 2022 / Accepted: 6 June 2022

Abstract
Coronavirus (COVID-19) creates an extensive range of respiratory contagions, and it is a kind of ribonucleic acid (RNA) virus, which affects both animals and humans. Moreover, COVID-19 is a new disease, which produces contamination in upper respiration alterritory and lungs. The new COVID is a rapidly spreading pathogen globally, and it threatens billions of humans' lives. However, it is significant to identify positive cases in order to avoid the spread of plague and to speedily treat infected patients. Hence, in this paper, the WSCA-based RMDL approach is devised for COVID-19 prediction by means of chest X-ray images. Moreover, Fuzzy Weighted Local Information C-Means (FWLICM) approach is devised in order to segment lung lobes. The developed FWLICM method is designed by modifying the Fuzzy Local Information C-Means (FLICM) technique. Additionally, random multimodel deep learning (RMDL) classifier is utilized for the COVID-19 prediction process. The new optimization approach, named water sine cosine algorithm (WSCA), is devised in order to obtain an effective prediction. The developed WSCA is newly designed by incorporating sine cosine algorithm (SCA) and water cycle algorithm (WCA). The developed WSCA-driven RMDL approach outperforms other COVID-19 prediction techniques with regard to accuracy, specificity, sensitivity, and dice score of 92.41%, 93.55%, 92.14%, and 90.02%.

Keywords COVID · Fuzzy local information c-means clustering · Random multimodel deep learning · Water cycle algorithm · Sine cosine algorithm

Introduction

The novel COVID disease is a severe deadly syndrome, which initiates from Wuhan territory, China, during December 2019 and spread worldwide [1]. The first case of COVID-19 is accounted in Wuhan, and it belongs to coronavirus (CoV) family, named as acute respiratory syndrome coronavirus 2 (SARS-CoV-2) prior it was known as COVID-19 through World Health Organization (WHO) in February 2020. The epidemic was confirmed by the Public Health Emergency of International Concern on 30 January 2020, and lastly, on March 11, 2020, WHO affirmed COVID-19 as a deadly disease [2]. After the epidemic, the amount of day-to-day cases started to enlarge exponentially and attained 1.8 million cases and approximately 114,698 demises in worldwide by 12 April 2020 [3]. Moreover, many CoV influence animals, although they can also be passed to humans due to their zoonotic character [4]. Besides, COVID-19 occurrence has been immense distress to the health community, since no successful treatment has been exposed [5–8]. The biological organization of COVID-19 includes positive-oriented single RNA, such that it is complex to treat sickness on account of its transforming nature. However, international medical specializations suffer exhaustive research to devise an effectual treatment for COVID disease. Nowadays, COVID-19 is a crucial reason for thousands of demises internationally, and more demises are in USA, Iran, Italy, UK, and Spain. In addition, numerous kinds of COVID are present, and these diseases are generally identi-

✉ R. Rajeswari
rajimaniphd@gmail.com

[1] Department of Electronics and Communication Engineering, Rajalakshmi Institute of Technology, Chennai, India

[2] Department of Computer Science and Engineering, Koneru Lakshmaiah Education Foundation, Vaddeswaram, Guntur, 522502 Andhra Pradesh, India

[3] Department of Computer Science and Engineering, Chitkara University Institute of Engineering and Technology, Chitkara University, Baddi, Himachal Pradesh, India

[4] Department of Computer Science and Engineering, GMR Institute of Technology, Rajam, Andhra Pradesh, India

Published online: 05 July 2022

fied in animals. Meanwhile, COVID-19 has been revealed in humans, bats, cats, pigs, rodents, dogs, poultry, and so on [1].

The characteristic clinical characteristics of COVID-19 contain cough, sore throat, muscle pain, fever, fatigue, headache, and lack of breath [4, 9]. Moreover, this virus can inflame the death of humans with destabilized immune systems [1, 10, 11]. Generally, COVID-19 is spread from one person to other person habitually through physical interaction. However, healthy people can be affected by hand, breath, or mucous contact with people, who have COVID-19 [1, 12]. The most general investigation approach presently utilized for COVID-19 detection is real-world reverse transcription polymerase chain reaction (RT-PCR). Additionally, chest radiological imaging, namely computed tomography (CT) and X-ray are very important parts of premature prediction and treatment of this disease [4, 13–15]. In general, X-ray images are recognized as effective for observing and evaluation of different lung illnesses, like pneumonia, tuberculosis, infiltration, and hernia. Meanwhile, COVID-19 is obvious as lung infection and upper respiratory tract, which was first examined in China in late 2019. Since, the virus has spread quickly, it becomes a global epidemic with more number of cases and deaths still growing [16]. Therefore, chest X-ray images are considered helpful, because COVID-19 affects lung tissues. Thus, X-ray images are also widely employed in order to detect COVID-19 disease [8].

In recent days, artificial intelligence (AI) is most commonly utilized for accelerating bio-medical researches [1]. Furthermore, the applications of machine learning techniques for automatic detection in medical fields are more attractive, and it is an effectual tool for physicians [4, 17–19]. Moreover, various deep learning techniques, and AI are widely employed for several applications, data classification, image detection, and segmentation of image [1, 20, 21]. However, the people, who are contaminated by COVID-19, may be affected by pneumonia owing to the virus spreading to the lungs. A greater number of deep learning methods have discovered the disease using X-ray images [1, 22]. The deep learning technique is the most familiar research field of AI, which enables end-to-end model development in order to obtain effective outcomes based on the input image. Moreover, deep learning schemes are effectively employed in numerous issues, like breast cancer [23], as well as skin cancer classification [24], arrhythmia recognition, brain disease detection, and pneumonia discovery from chest X-ray images, lung segmentation, and fundus image segmentation. Additionally, the speed increment of the COVID-19 pandemic demands the proficiency need in this medical area [4]. Furthermore, a deep learning system was introduced for automatic prediction of COVID-19 disease [4]. The CNN-based model called CoroDet is used in the automatic detection of COVID-19. Also, the fine-tuning, extraction of deep features, and end-to-end training are used in the effective detection of COVID-19 [25–27]. Moreover, the end-to-end model needs a raw chest X-ray images for prediction purposes. Meanwhile, this technique was trained with 125 chest X-ray images, which was not a standard structure [28, 29].

Motivation

COVID-19 is a new disease, which produces contamination in upper respiration alterritory and lungs. The COVID-19 prediction is significant, and the early detection is more essential to control the spread and death rate. The challenges experienced by the existing COVID-19 prediction techniques are deliberated as follows:

- The noises in the chest X-ray images may affect the accuracy of the COVID-19 detection.
- The lobar fissures may affect the accuracy of the lung lobe segmentation.
- In some methods, huge database handling was difficult.
- Some methods have high computational complexity, which may affect the detection performance.

The aforesaid challenges experienced by the existing COVID-19 prediction approaches are considered the motivation to devise the WSCA-based RMDL technique.

Contribution

The most important intension of this research is to devise COVID-19 detection using the developed WSCA-based RMDL approach. This COVID-19 prediction process comprises three phases, namely pre-processing, lung lobe segmentation, and COVID-19 prediction. Initially, the input X-ray image is obtained, and it is passed to the pre-processing stage. In the pre-processing stage, ROI extraction and Laplacian filtering are applied to remove the noises from the input image. Afterwards, lung lobe segmentation is done by the introduced FWLICM. The devised FWLICM is the modified approach of the FLICM technique [30]. After the lung lobe segmentation, COVID-19 prediction is done using the RMDL classifier [31]. Here, the RMDL is trained by the introduced WSCA for effectual classification performance. Furthermore, the devised WSCA is the incorporation of WCA [32] and SCA [33].

The most significant contribution of this research work is explicated as below:

- Developed WSCA-driven RMDL for COVID-19 prediction: The WSCA-based RMDL technique is introduced for the COVID-19 prediction process. Here, the RMDL classifier is utilized for predicting COVID-19 disease in which the RMDL is trained by the devised WSCA. Moreover, the introduced WSCA is newly developed by integrating SCA and WCA.

Research Questions

1. How the COVID-19 detection is done?
2. How the lung lobe segmentation is carried out?
3. How the training process of the RMDL is done for efficient COVID-19 prediction?
4. What is the purpose of integrating the SCA and WCA?

Literature Survey

The literature survey of the existing COVID prediction approaches with advantages and disadvantages are described in this section. Togacar [1] devised a support vector machine (SVM) for predicting COVID based on CT images. Here, fuzzy and stacking approaches were utilized for pre-processing the input chest image. Furthermore, social mimic optimization (SMO) algorithm was employed for the extraction of suitable features. This method improved the classification rate and reduced interference in each image. However, the resolution size of novel images, as well as organized images, must be similar. Ozturk et al. [4] modeled deep neural network (DNN) for COVID prediction by X-ray images. Moreover, this model developed a new deep learning system, termed DarkCovidNet structure for classification. This method offered precise detection for binary classification, although this model was not validated by including more images. Khan et al. [3] presented deep convolutional neural network (DCNN) technique for COVID prediction by means of the chest X-ray image. In addition, a transfer learning scheme was applied for initiating by weight parameters on huge databases. This prediction model obtained less computational cost, but still, only restricted amount of data was available in this method for the training process. Ismael and Sengur [34] developed SVM approach for COVID identification. Here, three DCNN techniques were applied in order to perform the prediction of COVID. Here, the cubic kernel function obtained better performance than other kernels in deep feature classification. Even though, an inadequate quantity of chest images was included in this approach for analysis process.

Pandit and Banday [35] introduced deep learning scheme for COVID prediction by X-ray images. This technique was robust and efficient of non-contact evaluation on COVID patients, and it assists for early and commercial prediction of COVID. However, this technique failed to evaluate by devising various optimization techniques. Autee et al. [36] presented multi-layer perceptron (MLP) stacked ensembling technique for COVID identification. Here, synthetic minority oversampling technique (SMOTE) was executed in order to reduce data imbalance issues. This technique increased accuracy and decreased false negative rate, but still, this approach needs more training time. Zhang et al. [37] devised two-step transfer learning structure for COVID prediction by X-ray images. This model obtained more precise performance of prediction, although it failed to evaluate the performance with more amount of chest X-ray images. Bassi and Attux [38] introduced the DCNN technique for predicting COVID using chest X-ray images. The classification performance of this approach was highly enhanced, even though the training process of this model was not effectual.

Proposed COVID-19 Identification Process Using Deep-Learning Method with Optimization Algorithm

This section explicates the developed WSCA-based RMDL approach for detecting COVID-19 by chest X-ray images. This COVID-19 detection technique mainly includes pre-processing, lung lobe segmentation, and COVID-19 prediction. At first, the input chest X-ray images are acquired from a dataset, and it is passed to the pre-processing step. The input image is pre-processed in order to remove the noises and redundant pixels using ROI extraction and Laplacian filtering model. After that, the lung lobes are segmented from the pre-processed image in the segmentation phase. The lung lobe segmentation is performed using the developed FWLICM technique. Finally, the COVID-19 detection process is done using the RMDL classifier [31], which is trained through the introduced WSCA. Moreover, the developed WSCA is introduced by combining SCA [39] and WCA [32] for effective prediction performance. The block diagram of the developed WSCA-based RMDL for COVID-19 prediction is depicted in Fig. 1.

Let us consider a dataset E with chest X-ray image, and it has p quantity of images, which is specified as,

$$\mathrm{E} = \left\{G_1, G_2, \ldots G_e, \ldots G_p\right\}, \tag{1}$$

where G_e denotes e^{th} image in a database, and p specifies the whole quantity of image in a database. Here, the input image G_e is considered, and it is fed to pre-processing phase.

Pre-processing

The pre-processing process is performed in order to reduce unnecessary pixels and noises available in an image. Here, the selected input chest image G_e is considered for pre-processing. The ROI extraction and Laplacian filtering are employed for eliminating the noises, such as salt and pepper noise, speckle noise, and Poisson noise from the input image.

ROI Extraction

The ROI in the chest X-ray image is determined based on pixel intensity value. In the ROI extraction process, concerned regions are separated from unresponsive regions for further

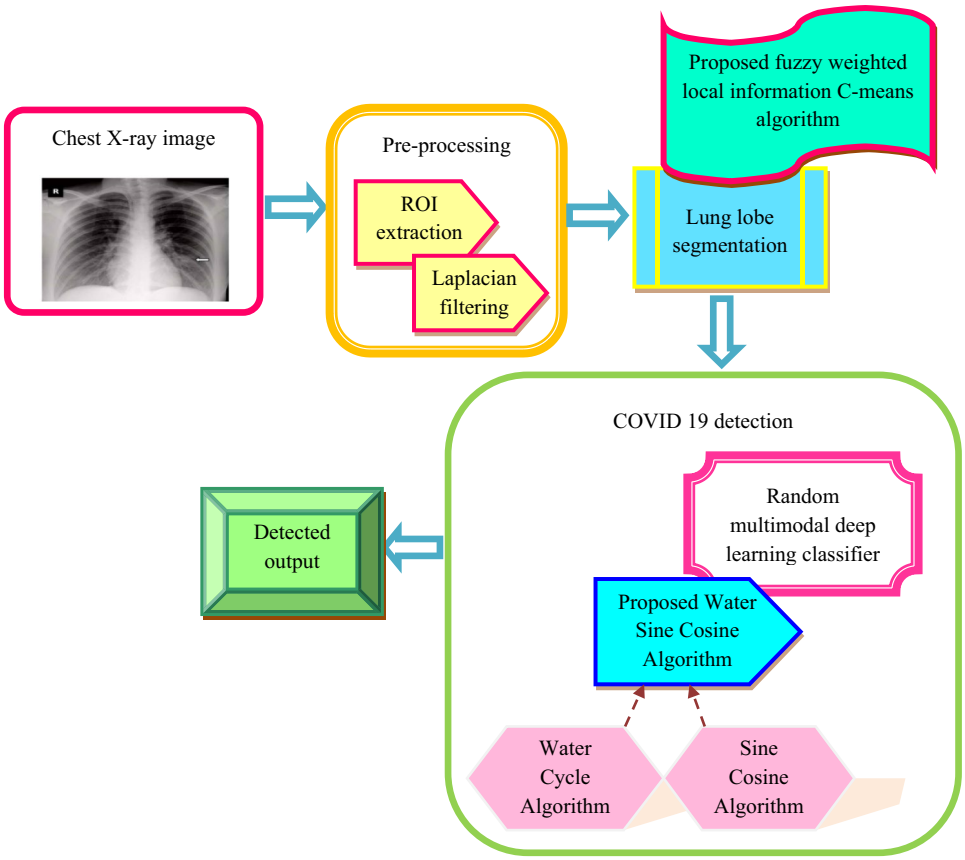

Fig. 1 Block diagram of the developed COVID-19 prediction using the developed WSCA-based RMDL algorithm

prediction process. The output from the ROI extraction process is represented as M_r.

Laplacian Filtering

Laplacian filter is an edge detector, which is employed to estimate second-order derivatives in an image. The Laplacian filter identifies the alternations in nearby pixels from continuous or edge progression. Therefore, Laplacian filtering is used for pre-processing in the COVID-19 prediction process. The output of Laplacian filtering is expressed as N_r. The output of pre-processed image is expressed as D_r.

Lung Lobe Segmentation by the Developed Fuzzy Weighted Local Information C-Means Algorithm

The pre-processed image D_r is considered the input for segmenting lung lobe segmentation. After the pre-processing of the input image, lung lobe segmentation process is performed for COVID-19 prediction. Here, the lung lobes are segmented using the FWLICM approach from the pre-processed image D_r. The FWLICM technique is designed by the modification of the FLICM technique [30], in which the Jaccard similarity coefficient is included in the FLICM technique. This method employs fuzzy local similarity measure, which offers assurance for image detail preservation and noise inventiveness. In FLICM [30], the weighted fuzzy factor is expressed as,

$$\mathrm{H}_{ql} = \sum_{\substack{k \in \mathrm{B}q \\ l \neq k}} \frac{1}{g_{lk}+1}\left(1-f_{qk}\right)^{\mathrm{I}} \|\mathrm{O}_k - \mathrm{P}_q\|^2 + \mathrm{Z}_{kq} \tag{2}$$

Here, Z_{kq} indicates Jaccard similarity coefficient, and it is estimated by,

$$\mathrm{Z}_{kq} = \frac{|\mathrm{K} \cap \mathrm{T}|}{|\mathrm{K} \cup \mathrm{T}|} \tag{3}$$

where $K = O_k$, $T = P_q$, the reference cluster is denoted as q, B refers whole pixel amount, k^{th} pixel with respect to amount of neighbors within the window around the q^{th} pixel B_q. P_q is the prototype of cluster center q, g_{lk} denotes the spatial Euclidean distance among pixels l and k, f_{qk} is the membership degree of k^{th} pixel in q^{th} cluster, and O_k is the gray-level value of k^{th} pixel.

Generally, the FLICM method combines local spatial as well as gray-level data to its objective function, which is given by,

$$A_I = \sum_{l=1}^{B}\sum_{q=1}^{d} f_{ql}^{I}\|O_l - P_q\|^2 + H_{ql} \quad (4)$$

where d is the cluster prototypes, the stopping criterion is I, the term O_l is a gray-level rate of the l^{th} pixel, and denotes weighted fuzzy factor.

The processes of FWLICM clustering are specified as below,

Step1: Let us consider cluster prototypes quantity c, fuzzification parameter I and stopping circumstance ρ.
Step2: Initialize the fuzzy partition matrix in random manner.
Step3: Fix loop counter as $\Upsilon = 0$.
Step4: Estimate cluster prototype by the following expression,

$$P_q = \frac{\sum_{l=1}^{B} f_{ql}^{I} O_l}{\sum_{l=1}^{B} f_{ql}^{I}} \quad (5)$$

Step5: Compute membership values by,

$$f_{ql} = \frac{1}{\sum_{k=1}^{d}\left(\frac{\|O_l - P_q\|^2 + H_{ql}}{\|O_l - P_q\|^2 + H_{kl}}\right)^{\frac{1}{I-1}}} \quad (6)$$

Step 6: If $\max\left\{X^p - X^{(p+1)}\right\} < \rho$, then discontinue the process, otherwise set $\Upsilon = \Upsilon + 1$ and go to step 4.

The outcome of lung lobe segmentation is denoted as L_s, and it is passed to deep learning classifier for predicting COVID.

COVID-19 Detection Based on Developed Water Sine Cosine Algorithm-Based Random Multimodel Deep Learning

This section explicates about the developed WSCA-based RMDL approach for COVID identification. The lung lobe segmented image L_s is taken as input for the COVID prediction process. Moreover, the RMDL classifier is trained by the developed optimization method, termed WSCA. However, the developed WSCA is devised by integrating SCA and WCA.

Random Multimodel Deep Learning for COVID Prediction

RMDL classifier [31] is a deep learning system, which is employed for effective COVID-19 prediction process. This RMDL includes deep recurrent neural networks (RNN), deep neural network (DNN), and deep convolutional neural network (CNN) blocks. The layer and node count of every deep learning multi-method are generated at random. The RMDL classifier effectively affords better performance in huge databases and easily solves classification issues. The architecture of the RMDL classifier is specified in Fig. 2.

Deep Neural Network

The DNN representation is introduced to learn various layer connections in which all layer receives connection based on prior parameters. Furthermore, it affords correlation to the successive layer of the hidden part. The input characterizes the feature involvement by the first hidden layer of every arbitrary method. Moreover, the output layer identifies several classes to execute multi class classification and obtains input for the binary classification process. All learning element is generated arbitrarily, and it uses the benchmark backpropagation method with activation and ReLU function in DNN. Thus, the activation function is specified as,

$$V(b) = \frac{1}{1 + e^{-b}} \in (0, 1) \quad (7)$$

$$V(b) = \max(0, b) \quad (8)$$

Moreover, the sigmoid function is illustrated as,

$$\upsilon(m)_t = \frac{e^{m_t}}{\sum_{n=1}^{N} e^{2n}} \quad (9)$$

where m_t denotes data point, and n specifies arbitrary integer, which lies from $1 \le n \le N$.

$$\forall t \in \{1 \ldots N\} \quad (10)$$

where N indicates the random number.

Recurrent Neural Network

The RNN distributes more weights before the data point sequence. Therefore, this approach is effective for identifying sequential data. In RNN, the neural network utilizes data of prior nodes for enhancing semantic assessment of database, which is specified by,

$$b_m = R\left(b_{m-1}, a_m, \varphi\right) \quad (11)$$

where b_m indicates state at time m, and a_m denotes input and time m. The weighting term is used for modeling the above equation,

$$b_m = F_{re}\nu(b_{m-1}) + F_{in}a_m + \kappa \quad (12)$$

where F_{re} is a recurrent matrix weight, F_{in} specifies input weight, κ denotes bias, and ν symbolizes element-wise function.

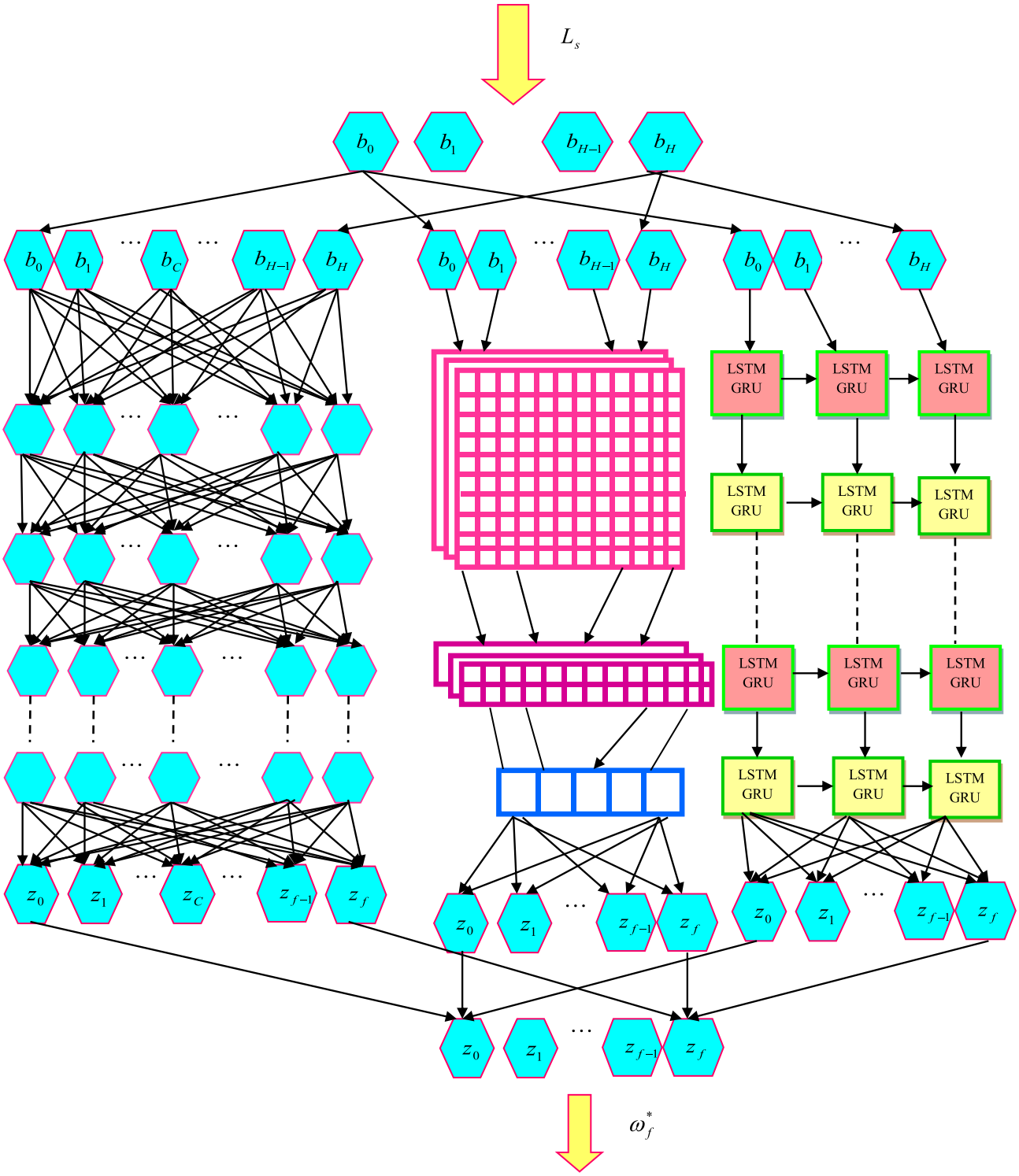

Fig. 2 Architecture of RMDL classifier

Long Short-Term Memory (LSTM)

LSTM is an exceptional structure of RNN, which conserves large dependencies in more effective way, and it is contrary to fundamental RNN. This is helpful to defeat the desertion gradient problems. However, LSTM is a chain-like system, which employs dissimilar gates to regulate quantity of data that are distributed to every node state.

The input gate is specified as,

$$C_m = \nu\left(\psi_C | b_m, Q_{m-1}\right) + \kappa_C \tag{13}$$

where ψ denotes weight matrices, b_m specifies input to the memory cell at time m, C is as input, and Q is a hidden layer.

After that, candid memory cell value is given by,

$$\overline{B}_m = \tanh\left(\psi_B | b_m, Q_{m-1}\right) + \kappa_B \tag{14}$$

Moreover, activation of the forget gate is illustrated by,

$$H_m = \nu\left(\psi_H | b_m, Q_{m-1}\right) + \kappa_H \tag{15}$$

Additionally, new memory cell value is expressed as,

$$B_m = C_m * \overline{B}_m + H_m B_{m-1} \tag{16}$$

Finally, the output gate is denoted as,

$$O_m = \nu\left(\psi_O | b_m, B_{m-1}\right) + \kappa_O \tag{17}$$

$$Z_m = O_m \tan\left(H_m\right) \tag{18}$$

Gated Recurrent Unit (GRU)

Generally, GRU is the gating approach of RNN, and it is considered a fundamental substitute method of the LSTM approach. GRU model includes two gates, and GRU where GRU does not have interior memory, and thus, non-linearity cannot be utilized. The specification of GRU cell is,

$$S_m = \nu_f\left(\psi_S b_m + I_z B_{m-1} + \kappa_S\right) \tag{19}$$

where S_m denotes the update gate vector of m, b_m is a input vector, ψ, I_z and κ refer to parameter matrices and vector, and ν_f signifies activation function, which can be ReLU or sigmoid.

$$Y_m = \nu_f\left(\psi_Y b_m + I_Y B_{m-1} + \kappa_Y\right) \tag{20}$$

$$Z_m = S_m \circ B_{m-1} + \left(1 - Y_m\right) \circ \nu_Z\left(\psi_B B_m\right) + I_B\left(Y_m . B_{m-1}\right) + \kappa_B \tag{21}$$

where Z_m indicates output vector of m, Y_m is a reset gate vector of m, S_m refers to update gate vector of m, and ν_Z represents the hyperbolic tangent function.

Convolutional Neural Network

The last deep learning model in RMDL is the CNN, which is modified to classify the input image. However, it is generated to process the images, and CNN is efficiently utilized to classify the image. In this, CNN is utilized to process image tensor that is convolved based on several kernel groups with $\omega \times \omega$. These convolutional layers are termed as feature maps, and it can be weighted to afford dissimilar filters on input. The CNN employed pooling model in order to decrease computation difficulty, and it decreased the output dimension from one layer to the next layer. Moreover, the general pooling approach is a max pooling in which the highest component is chosen from the pooling window. The maps are compressed to one column to supply the pooling outcome from the stacked featured maps to the final layer. Furthermore, the final layers of CNN are fully connected layers. Thus, the final classified output is represented as ω_f^*.

Developed Water Sine Cosine Algorithm for Training Process of Random Multimodel Deep Learning

This section illustrates the developed WSCA for the training procedure of RMDL. The RMDL is trained through the devised optimization model, termed WSCA, which is designed by SCA and WCA. WCA [32] is stimulated by the nature, and it is developed depending on the water cycle reflection and flowing of streams and river over sea in real-world circumstance. The WCA has the capacity to resolve different engineering enterprises and controlled optimization issues. Besides, WCA is effectual for affording qualitative solutions and provides effective computational efficiency. This approach is utilized to address everyday optimization problems with adequate solution accuracy. Moreover, it is effectual in managing dissimilar combinatorial optimization problems and offers the best solution with minimum computational complexities. SCA [39] is a population-based optimization approach in order to solve optimization issues. This method generates numerous early random candidate solutions and requests them to oscillate away or near optimal solutions based on scientific representation with cosine and sine functions. In addition, several adaptive and random variables are incorporated with the SCA algorithm for emphasizing exploitation and exploration of search space in different milestones of optimization. This algorithm successfully manages real-world problems with constrained and indefinite search space. Therefore, the SCA is combined with WCA to acquire enhanced performance. The algorithmic process of the developed WSCA is explicated as below.

Step-1: Initialization At first, populations of raindrops are generated arbitrarily, which is illustrated by,

$$K = \{K_1, K_2, \cdots, K_v, \cdots K_w\}; 1 \le v \le w \tag{22}$$

where w represents the whole amount of population, and K_v denotes the v^{th} population.

Step-2: Fitness Function Calculation The fitness measure is calculated for predicting the best solution for COVID prediction. The fitness with minimal rate is taken as an optimum solution, which is calculated as,

$$MSE = \frac{1}{h}\sum_{f=1}^{h}\left[\omega_f - \omega_f^*\right]^2 \tag{23}$$

where ω_f indicates the target output, ω_f^* specifies the classified output, and h denotes the total number of samples.

Step-3: Compute Every Raindrop Value Here, the cost of every raindrop is estimated by the following expression,

$$T_o = f\left(K_1^o, k_2^o, ...K_{w_{\text{var}}}^o\right); o = 1, 2, ...w_{pop} \tag{24}$$

where T_o is a cost of rain drop, w_{pop} specifies the amount of rain drops and w_{var} denotes the quantity of design variables.

Step-4: Estimation of Flow Strength for Sea and Rivers Here, flow power of river and sea is computed for assigning the raindrops, and it is calculated by,

$$wA_k = round\left(\left|\frac{T_j}{\sum_{j=1}^{w_{sr}} T_j}\right| \times w_{raindrops}\right) j = 1, 2, ...w_{sr} \tag{25}$$

where T_j symbolizes the amount of streams, which flow to specific sea or rivers.

Step-5: Stream Flow to River Once the flow concentration for river and sea is computed, then the stream flow to rivers is calculated as,

$$K_{stream}^{j+1} = K_{stream}^{j} + randx\left(K_{river}^{j} - K_{sream}^{j}\right) \tag{26}$$

Step-6: River Flow to Sea After calculation of the stream flow to river, the solution updation is carried out using the developed WSCA. In this step, river flow to sea is calculated, and its maximum downhill position by,

$$K_{river}^{j+1} = K_{river}^{j} + randx\left(K_{sea}^{j} - K_{river}^{j}\right) \tag{27}$$

$$K_{river}^{j+1} = K_{river}^{j}(1 - randx) + randxK_{sea}^{j} \tag{28}$$

Meanwhile, standard location update expression of SCA is,

$$K^{j+1} = K^j + y_1 \sin\left(y_2\right)\left|y_3 M_j - K_j\right| \tag{29}$$

Let us assume that $M_j > U_j$,

$$K^{j+1} = K^j + y_1 \sin\left(y_2\right)\left(y_3 M_j - K_j\right) \tag{30}$$

$$K^j = \frac{K^{j+1} - y_1 y_3 \sin\left(y_2\right) M_j}{1 - y_1 \sin\left(y_2\right)} \tag{31}$$

The above equation is rewritten as in terms of WCA, and thus, we get,

$$K^j = \frac{K_{river}^{j+1} - y_1 y_3 \sin\left(y_2\right) M_j}{1 - y_1 \sin\left(y_2\right)} \tag{32}$$

Substitute Eq. (32) in (28),

$$K_{river}^{j+1} = \frac{K_{river}^{j+1} - y_1 y_3 \sin\left(y_2\right) M_j}{1 - y_1 \sin\left(y_2\right)}(1 - randx) + randxK_{sea}^{j} \tag{33}$$

$$K_{river}^{j+1} = \frac{1 - y_1 \sin\left(y_2\right)}{randx - y_1 \sin\left(y_2\right)}\left[randxK_{sea}^{j} - \frac{y_1 y_3 \sin\left(y_2\right) M_j}{1 - y_1 \sin\left(y_2\right)}(1 - randx)\right] \tag{34}$$

Therefore, the aforementioned equation expresses the final updated equation for the introduced WSCA, where *rand* symbolizes evenly allocated random value ranges from 0 to 1, x is the value among 1 and 2, y_1, y_2, and y_3 are random numbers, and M_j represents destination point.

Step-7: Replace the Location of River Here, the river location is exchanged with stream and it provides an improved solution. Furthermore, if the river recognizes an optimal solution than the sea, then the position of the river is substituted with the sea.

Step-8: Evaporation Condition Evaporation is a significant aspect, which evades quick convergence in this approach. The evaporation condition is expressed as,

$$\left|k_{sea}^{j} - K_{river}^{j}\right| < T_{\max}; j = 1, 2, 3, ...w_{sr} - 1 \tag{35}$$

If directly above expression is fulfilled, then the training process is performed where $T_{\max}$ is a small value, which is near to zero.

Step-9: Raining Method After fulfillment of the evaporation situation, raining procedure is applied. The new location of produced streams is placed by,

$$K_{srteam}^{new} = LB + rand \times (UB - LB) \tag{36}$$

where *LB* and *UB* indicate lower and upper bound.

Additionally, computational performance, as well as convergence degree, is enhanced by the below expression, and it is only employed for stream, which directly flows to the sea.

$$K_{stream}^{new} = K_{sea} + \sqrt{\rho} randz\left(1, w_{\text{var}}\right) \tag{37}$$

where ρ represents coefficient, and it exposes the choice of searching zone near sea, and *randz* indicates arbitrarily allocated number.

Step-10: Reduce the Rate of User Define Parameter The big quantity of $T_{\max}$ decreases a search, whereas less rate supports search intensity nearby a sea. The worth of $T_{\max}$ is reduced as,

$$T_{\max}^{j+1} = T_{\max}^{j} - \frac{T_{\max}^{j}}{\max\ iteration} \tag{38}$$

Step-11: Check Possibility of Solution The best solution is calculated by the fitness function, and if the novel solution is improved than the former solution, then it updates the earlier value with the optimal one.

Step-12: Termination The aforementioned processes are repetitive until the best solution is attained for COVID prediction. The pseudocode of the developed WSCA is represented in Algorithm 1.

Algorithm 1 Pseudo code of the devised WSCA

Sl. No	Pseudo code of the introduced WSCA
1	**Input:** populace of rain drop and initial parameters
2	**Output:** best solution
3	Start
4	Initialize populace of rain drop, sea and river
5	Compute the fitness measure
6	Evaluate the price of every rain drop using expression (24)
7	Establish the strength of flow for rivers and sea using Eq. (25)
8	Stream flow to river is performed using expression (26)
9	River flow to sea is carried out through expression (34)
10	Replace the location of river and sea
11	Verify evaporation state
12	If $\left\|k_{sea}^{j} - K_{river}^{j}\right\| < T_{\max}; j = 1,2,3,...w_{sr} - 1$ do
13	Perform training procedure by means of expression (36) and (37)
14	**End if**
15	Replace user defined parameter
16	Verify the possibility of solution
17	**End**

Thus, the COVID-19 disease is predicted, and it obtains better performance by combining WCA with SCA.

Results and Discussion

The results and discussion of the introduced WSCA-driven RMDL approach for COVID prediction is displayed in this section. The experimental results, performance metrics, performance analysis, comparative approaches, experimental setup, comparative analysis, and comparative discussion are explicated in this section.

Experimental Setup

The implementation of the designed WSCA-based RMDL is executed based on MATLAB tool with Windows 10 OS, 8 GB RAM with Intel core-i3 processor, and the experimental setup is mentioned in Table 1.

Database Explanation

The execution of the designed WSCA-driven RMDL approach for COVID prediction is performed using DeepCovid Dataset [39]. This database mainly includes two folders, namely training and testing. This dataset contains 3100 test images and 2084 training images. In the training file, 84 images are COVID and 2000 images are non-COVID, whereas in the test set, 100 COVID images and 3000 images are non-COVID.

Performance Metrics

The performance of the introduced WSCA-driven RMDL scheme is computed by different metrics, like accuracy, specificity, sensitivity, and dice score.

Accuracy

Accuracy is employed to compute the true negative and true positive proportions of every sample, which is given by,

Table 1 Experimental setup

Parameter	Value
Batch size	128
Embedding dimension	50
Hidden layers of DNN	8
Hidden layers of RNN	5
Hidden layers of CNN	10
Number of iteration	100
Population size	10

$$Accuracy = \frac{E_o + E_g}{E_o + E_g + R_o + R_g} \tag{47}$$

Sensitivity

Sensitivity is a metric, which is calculated to predict the severity level of COVID disease, and it is specified as,

$$Sensitivity = \frac{E_g}{E_g + R_o} \tag{48}$$

Specificity

Specificity is estimated by precise identification of COVID, and it is expressed as,

$$Specificity = \frac{E_o}{E_o + R_g} \tag{49}$$

Dice Score

Dice score is estimated to quantify the performance of image segmentation methods, and it is expressed as,

$$Dice = \frac{2E_o}{2E_o + R_0 + R_g} \tag{50}$$

where E_o indicates true positive, E_g specifies true negative, R_o is a false positive, and R_g denotes false negative.

Experimental Outcomes

The experimental outcome of the devised WSCA-based RMDL model is displayed in this section. Here, the input chest X-ray image 1, 2, 3, and 4 are shown Fig. 3a in which image 1, 3, and 4 are non-COVID and image 2 is the COVID sample. The pre-processed image of input chest X-ray image 1, 2, 3, and 4 are portrayed in Fig. 3b. Moreover, the segmented image of the input chest X-ray image 1, 2, 3, and 4 are also portrayed in Fig. 3c.

Performance Analysis

The analysis of the WSCA-driven RMDL approach with different epoch sizes by varying k-fold and training data is specified in this section.

Analysis by Shifting Training Data

Table 2 exposes an analysis of the designed WSCA-driven RMDL by altering training data percentage by means of performance metrics. From this table, it is clear that the proposed system attains better performance when increasing the epoch and training data.

Performance Analysis by Changing K-fold

The performance analysis of the devised WSCA-driven RMDL by changing k-fold value based on performance metrics is specified in Table 3. The maximum accuracy, sensitivity, specificity, and dice score is attained at Epoch = 100 and the k-fold is 9.

Receiver-Operating Characteristic (ROC)-Based Performance Analysis

Table 4 depicts the ROC graph of performance analysis for the developed WSCA-based RMDL with different epoch sizes. The ROC analysis is an important tool for evaluating the diagnostic tests and predictive models. Also, it is utilized for assessing the accuracy quantitatively or compares accuracy between predictive or tests models. The developed WSCA-based RMDL model has TPR of 83.77%, 88.45%, 93.19%, and 93.93% for FPR of 20%, 40%, 60%, and 80% in epoch size 40. Similarly, the developed WSCA-based RMDL technique attains TPR value of 89.18%, 90.60%, 93.74%, 94.86%, 95.40%, 97.15%, 97.74%, 98.72%, and 100, while FPR is 20%, 30%, 40%, 50%, 60%, 70%, 80%, 90%, and 100% for the epoch size is 100.

Comparative Methods

The analysis of the introduced WSCA-driven RMDL approach is carried out by comparing the devised method with other conventional COVID prediction techniques, including deep learning [1], DNN [4], MLP [36], DCNN [38], and RNN [40].

Comparative Analysis

This section represents an analysis of the devised WSCA-based RMDL technique with regard to specificity, sensitivity, accuracy, and dice score by chaining k-fold and training data.

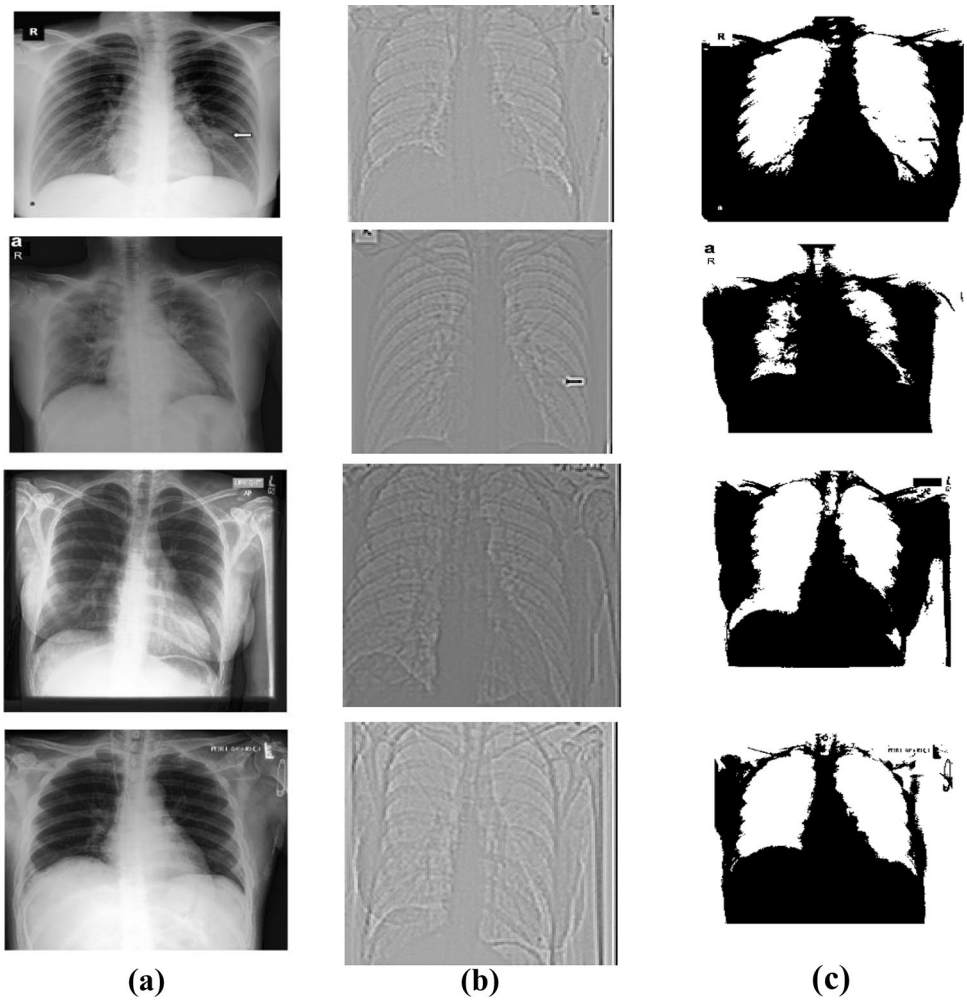

Fig. 3 Experimental outcomes of the developed WSCA-based RMDL **a** input image 1, 3, and 4 with non-COVID and input image-2 with COVID, **b** pre-processed image of input image 1, 2, 3, and 4, and **c** segmentation image of input image 1, 2, 3, and 4

Comparative Analysis by Altering Training Data Percentage

Table 5 denotes analysis of the devised WSCA-driven RMDL based on performance metrics by changing the training data. The developed WSCA-based RMDL obtained a better percentage improvement of 10.84%, 8.86%, 7.08%, 5.27%, and 3.55%, while compared with deep learning, DNN, MLP, RNN, and DCNN techniques for 80% training data. Similarly, the performance enhancement obtained by the designed WSCA-enabled RMDL is 12.31%, 9.62%, 8.45%, 6.44%, and 3.87% with other methods, like deep learning, DNN, MLP, RNN, and DCNN for the same training data. Likewise, the introduced WSCA-based RMDL attained better performance improvement of specificity for deep learning that is 15.26%, DNN is 13.33%, MLP is 9.47%, RNN is 8.14%, and DCNN is 5.29% for 80% training data. The proposed method has a maximum dice score of 89.20% for training data = 80%.

Comparative Analysis by Changing K-fold Value

Table 6 specifies analysis of the devised WSCA-driven RMDL based on performance metrics by varying k-fold. The accuracy obtained by the introduced WSCA-driven RMDL is 11.06%, 8.60%, 4.67%, 5.36%, and 2.36% performance improvement with other methods, like deep learning, DNN, MLP, RNN, and DCNN for considering k-fold = 8. Also, for the same k-fold, the devised WSCA-driven RMDL achieved better sensitivity percentage improvement of 13.78%, 7.79%, 4.36%, 4.77%, and 4.16%, while compared with deep learning, DNN, MLP, and DCNN methods. Similarly, the specificity value obtained by deep learning scheme is 77.26%, DNN is 79.31%, MLP is 84.88%, RNN is 86.21%, DCNN is 88.02%, and the developed WSCA-based RMDL is 89.78% for the k-fold value of 8. The proposed technique has a maximum dice score of 91.39, when k-fold = 8.

Table 2 Performance analysis of WSCA-driven RMDL by shifting training data percentage with various epoch size

Epoch/training data	20	40	60	80	100
	Accuracy (%)				
40	81.37	82.30	84.15	87.00	88.07
50	81.40	83.12	84.57	87.10	88.71
60	82.43	83.76	84.65	87.23	89.99
70	83.10	84.03	85.90	87.97	90.25
80	84.64	85.36	86.76	88.35	91.64
90	84.69	86.10	86.91	88.78	92.03
	Sensitivity (%)				
40	84.53	85.02	85.18	86.83	89.34
50	85.12	85.26	87.26	87.36	90.66
60	85.79	85.82	88.47	88.65	92.37
70	85.84	86.60	89.00	92.35	92.70
80	86.08	86.75	90.23	92.39	93.74
90	87.71	91.03	92.25	92.85	94.35
	Specificity (%)				
40	79.37	80.77	83.27	84.62	86.10
50	79.73	83.43	84.36	85.10	86.18
60	81.13	83.49	84.68	85.44	86.98
70	81.15	83.52	84.77	85.45	87.74
80	82.03	84.02	85.02	85.88	88.12
90	82.73	84.54	85.81	87.01	90.19
	Dice score (%)				
40	81.02	82.37	83.44	83.95	84.11
50	81.73	82.40	84.60	86.43	89.00
60	81.83	82.87	84.66	86.69	89.18
70	82.15	83.80	84.85	86.88	89.54
80	82.84	84.24	86.38	87.45	90.44
90	83.74	84.49	86.55	89.42	90.56

The training data, K-fold, and TPR values are represented in bold font

Table 3 Performance analysis of WSCA enabled RMDL by shifting k-fold value

Epoch/k-fold	20	40	60	80	100
	Accuracy (%)				
4	82.33	83.27	84.17	86.30	87.67
5	82.47	84.59	85.99	87.44	88.51
6	83.40	85.50	86.50	88.13	89.66
7	84.28	85.57	86.58	88.72	89.79
8	84.42	86.26	86.64	89.10	90.88
9	84.49	86.44	88.84	89.99	92.06
	Sensitivity (%)				
4	82.87	84.54	84.62	85.96	86.25
5	83.70	84.82	85.27	86.14	88.12
6	83.92	84.98	85.30	86.15	88.39
7	84.01	85.09	85.80	86.76	88.77
8	84.75	85.56	86.76	88.23	88.84
9	84.88	86.24	88.62	88.98	91.27
	Specificity (%)				
4	78.24	80.33	81.81	82.77	84.71
5	78.86	81.30	82.26	84.55	84.80
6	79.98	82.32	82.45	84.66	85.68
7	80.64	82.40	83.23	85.63	86.11
8	80.78	83.55	84.43	86.23	87.10
9	83.31	84.13	85.03	86.55	88.02
	Dice score (%)				
4	82.23	83.73	84.69	85.44	87.03
5	82.26	83.78	85.68	85.82	87.48
6	82.87	83.80	85.84	86.26	88.75
7	84.21	84.73	86.15	87.75	89.61
8	84.80	85.11	86.86	88.74	89.71
9	85.12	85.67	88.46	89.53	90.97

The training data, K-fold, and TPR values are represented in bold font

ROC-Based Comparative Analysis

Table 7 specifies the ROC graph of comparative analysis for the developed WSCA-based RMDL. The developed WSCA-based RMDL model has TPR of 75.32%, 77.57%, 79.82%, 83.24%, 86.21%, 89.26%, 90.80%, 91.28%, and 100%, while the FPR value is 20%. Similarly, when the FPR is 80%, the developed WSCA-based RMDL has TPR of 82.65%, 88.95%, 92.78%, 88.93%, 92.86%, 95.78%, 95.36%, 97.67%, and 100%.

Comparative Discussion

Table 8 specifies a comparative discussion of the devised WSCA-driven RMDL with other COVID prediction techniques by altering training data and k-fold value with performance metrics. The accuracy attained through deep learning, DNN, MLP, RNN, DCNN, and the developed WSCA-based RMDL is 82.59%, 84.43%, 87.98%, 89.1%, 90.48%, and 92.41% for the k-fold value of 9. Moreover, the sensitivity value of the developed WSCA-based RMDL approach is 92.58%, whereas deep learning model is 82.23%, DNN is 85.22%, MLP is 87.97%, RNN is 88.2%, and DCNN is 88.46% in the k-fold value of 9. When the f-fold value is 9, the specificity value of the deep learning method is 78.75%, DNN is 80.49%, MLP is 86.49%, RNN is 87.23%, DCNN is 89.07%, while the developed WSCA-based RMDL approach attains 92.14%. From the below discussion table, it is well noted that the introduced WSCA-based RMDL achieved an improved performance with accuracy and specificity of 92.41% and 92.14% in the k-fold value of 9 as well as the sensitivity of 93.55% in 90% of the training data. The proposed WSCA-based RMDL achieved a maximum dice score of 89.99% and 92.02% for varying the training data and k-fold, respectively.

The computational time of the devised and existing methods is depicted in Table 9. From this table, it is clear that the devised method has a minimum computational time of 140 s.

Table 4 ROC performance analysis for the developed WSCA-based RMDL

Epoch/TPR	Deep learning	DNN	MLP	RNN	DCNN	Developed WSCA-based RMDL
10	0	0	0	0	0	0
20	83.37	83.77	84.26	82.01	85.62	89.18
30	86.11	86.37	86.97	86.13	89.05	90.60
40	87.40	88.45	89.23	91.23	91.16	93.74
50	87.61	88.69	93.16	89.71	94.02	94.86
60	91.54	93.19	94.30	91.31	94.44	95.40
70	92.87	93.55	94.81	93.17	96.63	97.15
80	93.30	93.93	95.85	94.31	97.38	97.74
90	93.76	94.05	98.39	96.88	98.67	98.72
100	100	100	100	100	100	100

The training data, K-fold, and TPR values are represented in bold font

Table 5 Analysis of the devised WSCA-driven RMDL based on training percentage

Methods	Deep learning	DNN	MLP	RNN	DCNN	Developed WSCA-based RMDL
	Accuracy (%)					
40	76.24	78.67	80.82	82.2	84.53	87.08
50	77.36	80.50	81.64	82.3	85.45	88.12
60	78.05	80.60	83.38	84.0	85.71	88.42
70	78.92	81.93	83.47	84.5	85.83	88.88
80	80.19	81.97	83.57	85.2	86.74	89.94
90	81.68	82.94	83.86	86.3	88.08	90.60
	Sensitivity (%)					
40	77.83	79.62	83.17	83.5	83.84	89.93
50	78.20	81.82	83.65	84.1	85.65	90.10
60	80.26	82.79	83.95	85.3	87.31	91.46
70	80.59	83.11	83.99	85.8	87.57	91.85
80	80.97	83.46	84.54	86.4	88.77	92.35
90	82.68	84.46	85.26	87.3	90.46	93.55
	Specificity (%)					
40	76.31	76.75	79.70	80.2	80.75	85.63
50	76.45	78.18	80.54	81.3	82.77	87.22
60	77.37	78.27	81.33	82.4	86.03	89.39
70	77.44	78.45	81.34	83.3	86.27	90.71
80	77.58	79.35	82.88	84.1	86.70	91.55
90	79.18	80.34	85.10	86.3	87.18	91.55
	Dice score (%)					
40	75.74	76.71	79.38	81.61	82.27	86.60
50	75.94	79.12	79.49	81.74	82.99	86.63
60	76.50	79.12	81.45	83.21	84.07	87.10
70	77.07	79.25	81.92	83.64	84.12	88.40
80	77.89	80.13	82.77	84.12	85.14	89.20
90	78.05	80.69	83.76	84.62	87.34	89.99

The training data, K-fold, and TPR values are represented in bold font

Table 6 Comparative analysis of the designed WSCA-driven RMDL based on k-fold

Methods/K-fold	Deep learning	DNN	MLP	RNN	DCNN	developed WSCA-based RMDL
	Accuracy (%)					
4	75.27	78.80	81.36	81.4	81.57	84.21
5	76.53	78.87	82.31	83.6	86.04	89.23
6	76.95	80.26	82.49	84.1	86.68	89.36
7	78.13	81.17	83.30	85.1	87.15	90.20
8	80.70	82.94	85.87	86.5	88.60	90.74
9	82.59	84.43	87.98	89.1	90.48	92.41
	Sensitivity (%)					
4	76.56	81.55	82.86	83.0	83.23	85.63
5	76.60	83.36	84.20	84.3	84.42	85.94
6	77.98	83.67	84.36	85.0	85.40	86.14
7	78.46	83.91	85.79	86.0	86.32	90.80
8	78.52	83.98	86.72	87.1	87.28	91.07
9	82.23	85.22	87.97	88.2	88.46	92.58
	Specificity (%)					
4	74.93	77.61	83.08	83.51	84.19	84.81
5	75.03	77.98	83.22	84.61	85.53	87.83
6	75.72	78.06	83.75	85.41	87.29	88.62
7	76.79	79.22	84.38	85.63	87.71	89.45
8	77.26	79.31	84.88	86.21	88.02	89.78
9	78.75	80.49	86.49	87.23	89.07	92.14
	Dice score (%)					
4	74.37	76.04	79.87	80.12	81.14	85.77
5	74.42	76.69	80.71	81.33	82.06	87.48
6	74.49	77.08	80.80	81.54	82.11	88.70
7	75.82	77.76	81.44	81.67	82.59	89.54
8	76.78	80.10	82.71	83.23	84.85	91.39
9	79.39	80.70	83.98	85.34	88.22	92.02

The training data, K-fold, and TPR values are represented in bold font

Table 7 ROC comparative analysis for the developed WSCA-based RMDL

Methods/TPR	Deep learning	DNN	MLP	RNN	DCNN	Developed WSCA-based RMDL
10	0	0	0	0	0	0
20	75.32	76.58	81.54	82.01	82.65	82.66
30	77.57	79.99	85.01	86.13	88.95	91.00
40	79.82	81.17	89.33	91.23	92.78	93.84
50	83.24	85.71	89.81	89.71	88.93	95.70
60	86.21	87.97	90.31	91.31	92.86	94.32
70	89.26	90.25	92.46	93.17	95.78	96.59
80	90.80	91.06	93.56	94.31	95.36	97.45
90	91.28	94.06	96.56	96.88	97.67	99.45
100	100	100	100	100	100	100

The training data, K-fold, and TPR values are represented in bold font

Table 8 Comparative discussion

By changing	Metrics/methods	Deep learning	DNN	MLP	RNN	DCNN	Proposed WSCA-based RMDL
Training data percentage	**Accuracy (%)**	81.68	82.94	83.86	86.3	88.08	90.60
	Sensitivity (%)	82.68	84.46	85.26	87.3	90.46	**93.55**
	Specificity (%)	79.18	80.34	85.10	86.3	87.18	91.95
	Dice score (%)	78.05	80.69	83.76	84.62	87.34	89.99
K-fold value	**Accuracy (%)**	82.59	84.43	87.98	89.1	90.48	**92.41**
	Sensitivity (%)	82.23	85.22	87.97	88.2	88.46	92.58
	Specificity (%)	78.75	80.49	86.49	87.23	89.07	**92.14**
	Dice score (%)	79.39	80.70	83.98	85.34	88.22	**92.02**

The better performance results are represented using bold fonts

Table 9 Computational time

Methods	Deep learning	DNN	MLP	RNN	DCNN	Proposed WSCA-based RMDL
Computational time (sec)	325	310	288	256	241	**140**

The better performance results are represented using bold fonts

Conclusion

This paper presents and develop the WSCA-based RMDL approach for predicting COVID. Here, the chest X-ray image is considered an input for COVID prediction. This COVID performs the pre-processing process in order to eradicate the unrequited pixels and noises available in the input image. The ROI extraction and Laplacian filter are employed in order to eliminate the redundant pixels from the input image. The segmentation process is necessary in the prediction system for effective classification. Moreover, the FWLICM technique is devised for segmenting lung lobes from the pre-processed image. Here, the developed FWILCM is designed by the modification of the FLICM technique. Meanwhile, the RMDL classifier is employed for the prediction process of COVID. In addition, RMDL is trained through an introduced optimization approach, termed WSCA to achieve effective performance. However, the developed WSCA is newly developed by combining SCA and WCA. Moreover, the performance of the devised WSCA-enabled RMDL is evaluated by means of four metrics, like accuracy, sensitivity, specificity, and dice score. The introduced COVID prediction model achieves better performance with accuracy of 92.41%, sensitivity of 93.55%, specificity of 92.14%, and dice score of 92.02%. However, the classification of COVID-19 is not possible in the proposed method. In the future, hybrid deep learning classifier will be proposed for classifying the COVID-19 chest X-ray images.

Author Contribution R. Rajeswari conceived the presented idea and designed the analysis. Also, she carried out the experiment and wrote the manuscript with support from Dr. Veerraju Gampala, Balajee Maram, and R. Cristin. All authors discussed the results and contributed to the final manuscript. All authors read and approved the final manuscript.

Data Availability The dataset analysed during the current study is available in the DeepCovid Dataset repository, https://github.com/shervinmin/DeepCovid.

Declarations

Ethics Approval This paper does not contain any studies with human participants or animals performed by any of the authors.

Consent to Participate Not applicable.

Consent for Publication Not applicable.

Competing Interests The authors declare no competing interests.

References

1. Togacar, M., Ergen, B. and Cömert, Z., "COVID-19 detection using deep learning models to exploit Social Mimic Optimization and structured chest X-ray images using fuzzy color and stacking approaches", Computers in biology and medicine, vol.121, pp.103805, 2020.
2. Rupapara V, Narra M, Gunda NK, Gandhi S, Thipparthy KR: Maintaining Social Distancing in Pandemic Using Smartphones With Acoustic Waves. IEEE Transact Computation Soc Syst 1–7,2021
3. Khan AI, Shah JL, Bhat MM: CoroNet: A deep neural network for detection and diagnosis of COVID-19 from chest x-ray images. Comp Methods Prog Biomed 196:105581,2020
4. Ozturk T, Talo M, Yildirim EA, Baloglu UB, Yildirim O, Acharya UR: Automated detection of COVID-19 cases using deep neural networks with X-ray images. Comput Biol Med 121:103792,2020
5. Mangal A, Kalia S, Rajgopal H, Rangarajan K, Namboodiri V, Banerjee S, Arora C: CovidAID: COVID-19 detection using chest X-ray. arXiv preprint https://arxiv.org/abs/2004.09803. 2020

6. Dev K, Khowaja SA, Jaiswal A, Bist AS, Saini V, Bhatia S: "Triage of Potential COVID-19 Patients from Chest X-ray Images using Hierarchical Convolutional Networks. arXiv preprint https://arxiv.org/abs/2011.00618. 2020.
7. Qiao Z, Bae A, Glass LM, Xiao C, Sun J: FLANNEL: Focal Loss Based Neural Network Ensemble for COVID-19 Detection. arXiv preprint https://arxiv.org/abs/2010.16039, 2020.
8. Rothe C, Schunk M, Sothmann P, Bretzel G, Froeschl G, Wallrauch C, Zimmer T, Thiel V, Janke C, Guggemos W, Seilmaier M: Transmission of 2019-nCoV infection from an asymptomatic contact in Germany. New England J Med 382(10):970-971,2020.
9. Singhal T: A review of coronavirus disease-2019 (COVID-19). The Indian J Pedriatics 87(4):281-286,2020.
10. Lancet T: COVID-19: too little, too late?. Lancet (London, England) 395(10226):755, 2020.
11. Razai MS, Doerholt K, Ladhani S, Oakeshott P: Coronavirus disease 2019 (covid-19): a guide for UK GPs. BMJ 368,2020.
12. Peng X, Xu X, Li Y, Cheng L, Zhou X, Ren B: Transmission routes of 2019-nCoV and controls in dental practice. Int J Oral Sci 12(1):1-6,2020.
13. Zu ZY, Jiang MD, Xu PP, Chen W, Ni QQ, Lu GM, Zhang LJ: Coronavirus disease 2019 (COVID-19): a perspective from China. Radiology 296(2):E15-E25,2020.
14. Fusini F, Bisicchia S, Bottegoni C, Gigante A, Zanchini F, Busilacchi A: Nutraceutical supplement in the management of tendinopathies: a systematic review. Muscles, Ligaments Tendons J 6(1):48-57,2016.
15. Catani O, Cautiero G, Sergio F, Cattolico A, Calafiore D, de Sire A, Zanchini F: Medial Displacement Calcaneal Osteotomy for Unilateral Adult Acquired Flatfoot: Effects of Minimally Invasive Surgery on Pain, Alignment, Functioning, and Quality of Life. The J Foot Ankle Surge 60(2):358-361,2021.
16. Abolfazl Zargari Khuzani, Morteza Heidari, and S. Ali Shariati, "COVID-Classifier: an automated machine learning model to assist in the diagnosis of COVID-19 infection in chest X-ray images," Scientific Reports, vol. 11, 2021.
17. Litjens G, Kooi T, Bejnordi BE, Setio AAA, Ciompi F, Ghafoorian M, Van Der Laak JA, Van Ginneken B, Sánchez CI: A survey on deep learning in medical image analysis. Med Image Anal 42:60-88,2017.
18. Ker J, Wang L, Rao J, Lim T: Deep learning applications in medical image analysis. IEE Access 6:9375-9389,2017.
19. Faust O, Hagiwara Y, Hong TJ, Lih OS, Acharya UR: Deep learning for healthcare applications based on physiological signals: A review. Comput Methods Programs Biomed 161:1-13,2018.
20. Toğaçar M, Ergen B, Cömert Z: Application of breast cancer diagnosis based on a combination of convolutional neural networks, ridge regression and linear discriminant analysis using invasive breast cancer images processed with autoencoders. Med Hypotheses 135:109503
21. Liu X, Deng Z, Yang Y: Recent progress in semantic image segmentation. AI Intel Rev 52(2):1089-1106,2019.
22. Jaiswal AK, Tiwari P, Kumar S, Gupta D, Khanna A, Rodrigues JJ: Identifying pneumonia in chest X-rays: A deep learning approach. Measurement 145:511-518,2019.
23. Vinolin V: Breast Cancer Detection by Optimal Classification using GWO Algorithm. Multimedia Res 2(2)10-18,2019.
24. Ganeshan R: Skin Cancer Detection with Optimized Neural Network via Hybrid Algorithm. Multimedia Res 3(2):27-34,2020.
25. Tahamtan A, Ardebili A: Real-time RT-PCR in COVID-19 detection: issues affecting the results. Expe Rev Mole Diagnost 20(5):453-454,2020.
26. Ismael AM, Şengür A: Deep learning approaches for COVID-19 detection based on chest X-ray images. Exp Syst App 164,2021.
27. Hussain E, Hasan M, Rahman A, Lee I, Tamanna T, Parvez MZ: CoroDet: A deep learning based classification for COVID-19 detection using chest X-ray images. 142, 2021.
28. Purohit K, Kesarwani A, Kisku DR, Dalui M: Covid-19 detection on chest x-ray and ct scan images using multi-image augmented deep learning model. BioRxiv, 2020.
29. Ahmed S, Hossain T, Hoque OB, Sarker S, Rahman S, Shah FM: Automated COVID-19 Detection from Chest X-Ray Images: .A High Resolution Network (HRNet) Approach. medRxiv, 2020.
30. Krinidis S, Chatzis V: A robust fuzzy local information C-means clustering algorithm. IEEE Transact Image Process 19(5):1328-1337,2010.
31. Kowsari K, Heidarysafa M, Brown DE, Meimandi KJ, Barnes LE: Rmdl: Random multimodel deep learning for classification. In Proc 2nd Int Conf Inform Syst Data Mining 19–28,2018.
32. Eskandar H, Sadollah A, Bahreininejad A, Hamdi M: Water cycle algorithm–A novel metaheuristic optimization method for solving constrained engineering optimization problems. Comp Struct 110:151-166,2012.
33. Mirjalili S: SCA: a sine cosine algorithm for solving optimization problems. Knowledge-based Syst 96:120-133,2016.
34. Ismael AM, Sengur A: Deep learning approaches for COVID-19 detection based on chest X-ray images. Expert Syst App 164:114054,2021.
35. Pandit MK, Banday SA: SARS n-CoV2–19 detection from chest x-ray images using deep neural networks. Int J Pervasive Comput Commun 2020.
36. Autee P, Bagwe S, Shah V, Srivastava K: StackNet-DenVIS: a multi-layer perceptron stacked ensembling approach for COVID-19 detection using X-ray images: Phys Eng Sci Med 43(4):1399-1414, 2020.
37. Zhang R, Guo Z, Sun Y, Lu Q, Xu Z, Yao Z, Duan M, Liu S, Ren Y, Huang L, Zhou F: COVID19XrayNet: A Two-Step Transfer Learning Model for the COVID-19 Detecting Problem Based on a Limited Number of Chest X-Ray Images. Interdis Sci Computl Life Sci 12(4):555-565,2020.
38. Bassi PR, Attux R: A deep convolutional neural network for covid-19 detection using chest x-rays. arXiv preprint https://arxiv.org/abs/2005.01578. 2020.
39. DeepCovid Dataset: https://github.com/shervinmin/DeepCovid. Accessed on February 2021.
40. Hassan A, Shahin I, Bader M: COVID-19 Detection System Using Recurrent Neural Networks. In the Proc Int Conf Commun, Comput, Cybersec Informat 2020